

Analysis of Heterogeneous Vehicular Traffic: Using Proportional Densities

Nanyondo Josephine^{a,b,*}, Henry Kasumba^b

^a*Department of Mathematics, Faculty of Science and Education, Busitema University, P.O Box 236, Tororo, Uganda*

^b*Department of Mathematics, School of Physical Sciences, Makerere University, P.O Box 7062, Kampala, Uganda*

Abstract

An extended multi-class Aw-Rascole (AR) model with pressure term described as a function of area occupancy defined in form of proportional densities is presented. Two vehicle classes that is; cars and motorcycles are considered based on an assumption that proportions of these form total traffic density. Qualitative properties of the proposed equilibrium velocity is established. Conditions under which the proposed model is stable are determined by linear stability analysis. To compute numerical flux, the model is discretized by the original Roe decomposition scheme, where Roe matrix, averaged data variables and wave strengths are explicitly derived. The Roe matrix is shown to be hyperbolic, consistent and conservative. From the numerical results, the effect of motorcycles proportion on the flow of vehicle classes is determined. Results obtained remain within limits therefore, the proposed model is realistic.

Keywords: Multi-class, Roe decomposition, heterogeneous traffic, area occupancy, macroscopic, Aw-Rascole model, proportional densities

1. Introduction

In developing countries, various vehicle classes use same roads at the same time. This is why traffic flow models that combine vehicle classes are necessary in the study of heterogeneous vehicular traffic flow. The traffic flow models are classified as macroscopic, microscopic or mesoscopic. Macroscopic models consider traffic flow as a compressible fluid formed by vehicles [1] and capture general relationship between flow, density and velocity of vehicles [2, 3]. Microscopic models describe interactions between vehicles within a traffic stream [4, 5]. The microscopic models consider characteristics such as; vehicle lengths, speeds, accelerations, time, space headways, vehicle and engine capabilities and human characteristics that describe the driving behaviors. Mesoscopic models are described by a combination of microscopic and macroscopic characteristics through probability distributions [2] but at a high level of aggregation usually by speed-density relations and queuing theory approaches [3].

*This article is a result of the PhD program funded by Makerere-Sida Bilateral Program under Project 316 "Capacity Building in Mathematics and Its Applications".

*Corresponding author

Email addresses: jnanyondo@sci.busitema.ac.ug (Nanyondo Josephine), kasumba@cns.mak.ac.ug (Henry Kasumba)

2020 Mathematics subject classification: 05C50

Traffic flow is either homogeneous, heterogeneous, equilibrium or non-equilibrium. In homogeneous traffic, all vehicles follow lane discipline whereas in heterogeneous traffic, vehicles violate lane discipline. Equilibrium flow is characterized by constant velocity and spatial homogeneity. Whereas, non-equilibrium traffic flow is characterized by changes in both velocity and spatial homogeneity [2].

The macroscopic models are adopted because of their low computation complexity. The first macroscopic model was proposed by [6] and [7], given by

$$\frac{\partial \rho}{\partial t} + \frac{\partial(\rho v)}{\partial x} = 0.$$

To address the drawbacks of the first order methods in characterizing overtaking and creeping some researchers (see for example, [8] and the references therein) used various forms of definitions of the velocity function (in static form) together with the equation for the conservation of mass. However, the exact formulation of the velocity function for each class of vehicles is a challenge. Using the porous flow approach, Nair et al [9] formulated a multi-class heterogeneous traffic flow model using first order methods. The same theory is applied also in [10, 11] to formulate a model for heterogeneous traffic flow that takes overtaking and creeping into account. Since these models are based on the first order method they may fail to characterize some important traffic phenomena that occurs in heterogeneous traffic flow, like, stop and go wave, hysteresis [5], platoon dispersion [12].

Second and higher order models combine the dynamics of the velocity function together with the conservation equation of vehicles. For instance Payne [13, 14] has shown that the microscopic car-following model can only be generalized by a second and higher order continuum models. Gupta and Dhiman [15] have shown that a heterogeneous continuum second order model generalizes a kinematic car-following model for a non lane-based system of traffic flow that takes lateral separation into account. However, in their model, Gupta and Dhiman used the same equilibrium velocity for all vehicle classes. In order to characterize the phenomena of creeping (or gap filling), Mohan and Ramadurai [12, 16] used lateral area occupancy method to analyze the flow of heterogeneous traffic. However, they ignored the concept of proportional densities and their effect on the flow of vehicle classes.

In this paper, the effect of motorcycles proportion on the flow of vehicle classes is determined. The subsequent subsections of the paper are organized as follows. Derivation of area occupancy defined in terms of proportional densities and conservative form of the proposed model are shown in Section 2. In Section 3, qualitative properties of equilibrium velocity are discussed. A discretization scheme, Quasi-linear form, original Roe numerical scheme in which Roe matrix, averaged data variables, wave strengths and entropy condition are shown in Section 4. Stability analysis of the proposed model equations is done in Section 5. Numerical results are shown in Section 6. Finally, Section 7 draws conclusion on the paper.

2. Model formulation

In this section, the Aw-Rascle model is modified by introducing an area occupancy that is expressed in terms of vehicle class proportions and other lateral parameters in the pressure term.

2.1. ~~Ab~~ffic

We then introduce area occupancy (AO) that is defined in terms of proportional densities and derive it as follows. Suppose that the total density, ρ of vehicles that are occupying the road, at any time is given by

$$\rho = \rho_m + \rho_c, \quad (1)$$

where ρ_c refers to density of cars and ρ_m density of motorcycles. Let

$$\rho_m = \delta(\rho_m + \rho_c) = \delta\rho, \quad (2)$$

where δ represents the proportion of motorcycles that contribute to the total vehicular density on a given road section. Then

$$\rho_m = \frac{\delta\rho_c}{1-\delta}. \quad (3)$$

Assuming that the width of a motorcycle is one third the width of a car and considering l, w to be length and width of vehicles, the equation for area occupancy becomes

$$AO = \frac{\sum_i \rho_i a_i}{W} = \frac{\rho_c a_c + \rho_m a_m}{W} = \frac{(1-\delta)\rho a_c + \delta\rho a_m}{W}, \quad i = c, m. \quad (4)$$

Substitution of (3) into (4) leads to

$$AO = \frac{1}{W} \left(\rho_c a_c + \frac{\delta\rho_c a_m}{1-\delta} \right) = \frac{\rho_c [(1-\delta)a_c + \delta a_m]}{W(1-\delta)}, \quad (5)$$

where $a_i = l_i \times w_i$. Further simplification yields

$$\begin{aligned} AO &= \frac{(1-\delta)\rho_c l_c w_c + \delta\rho_c l_m w_m}{W(1-\delta)}, \quad w_m = \frac{1}{3}w_c, \\ &= \frac{\rho_c w_c}{W(1-\delta)} \left((1-\delta)l_c + \frac{1}{3}\delta l_m \right), \\ &= \rho_c \psi_c, \end{aligned} \quad (6)$$

where

$$\psi_c = \frac{w_c}{W(1-\delta)} \left((1-\delta)l_c + \frac{1}{3}\delta l_m \right), \quad (7)$$

and AO refers to area occupancy expressed in terms of proportional densities. Equivalently, AO can be rewritten as

$$\begin{aligned} AO &= \frac{\rho_m w_c (l_c(1-\delta) + \frac{1}{3}\delta l_m)}{W\delta}, \\ &= \rho_m \psi_m, \end{aligned} \quad (8)$$

where

$$\psi_m = \frac{w_c(l_c(1-\delta) + \frac{1}{3}\delta l_m)}{W\delta}. \quad (9)$$

60 It can be inferred from (3) that

$$\rho_c = \frac{\rho_m(1-\delta)}{\delta} = (1-\delta)\rho. \quad (10)$$

Consequently the total density in (1) then becomes

$$\rho = \rho_m + \rho_c = \delta\rho + (1-\delta)\rho.$$

Incorporating the two vehicle classes in AR model, we obtain the following proposed model

$$\left\{ \begin{array}{l} \frac{\partial \rho_m}{\partial t} + \frac{\partial (\rho_m v_m)}{\partial x} = 0, \\ \frac{\partial (v_m + p_m)}{\partial t} + v_m \frac{\partial (v_m + p_m)}{\partial x} = \frac{1}{\tau_m} (v_{em} - v_m), \\ \frac{\partial \rho_c}{\partial t} + \frac{\partial (\rho_c v_c)}{\partial x} = 0, \\ \frac{\partial (v_c + p_c)}{\partial t} + v_c \frac{\partial (v_c + p_c)}{\partial x} = \frac{1}{\tau_c} (v_{ec} - v_c), \end{array} \right. \quad (11)$$

where the respective pressure terms are given by

$$p_m = (\psi_m \rho_m)^{\gamma_m} \quad \text{and} \quad p_c = (\psi_c \rho_c)^{\gamma_c}.$$

65 Here ψ_m , ψ_c are parameters defined as in (7), (9) and γ_m , γ_c represent the relaxation time of motorcycles and cars, respectively.

We can express (11) in conservative form given by

$$\left\{ \begin{array}{l} \frac{\partial \rho_m}{\partial t} + \frac{\partial (\rho_m v_m)}{\partial x} = 0, \\ \frac{\partial (\rho_m (v_m + p_m))}{\partial t} + \frac{\partial (\rho_m v_m (v_m + p_m))}{\partial x} = \frac{\rho_m}{\tau_m} (v_{em} - v_m), \\ \frac{\partial \rho_c}{\partial t} + \frac{\partial (\rho_c v_c)}{\partial x} = 0, \\ \frac{\partial (\rho_c (v_c + p_c))}{\partial t} + \frac{\partial (\rho_c v_c (v_c + p_c))}{\partial x} = \frac{\rho_c}{\tau_c} (v_{ec} - v_c). \end{array} \right. \quad (12)$$

where the conserved variables are ρ_c , $\rho_c (v_c + p_c)$, ρ_m and $\rho_m (v_m + p_m)$,

Considering terms in system (12) with subscript c , let the generalized momentum be X_c , such that

$$X_c = \rho_c (v_c + p_c). \quad (13)$$

Rearranging terms in (13) we obtain

$$\frac{X_c}{\rho_c} = (v_c + p_c), \quad \text{and} \quad \rho_c v_c = X_c - \rho_c p_c.$$

70 This implies

$$\rho_c v_c (v_c + p_c) = (X_c - \rho_c p_c) \frac{X_c}{\rho_c},$$

which simplifies into

$$\frac{X_c^2}{\rho_c} - p_c X_c.$$

The same is done on terms with subscript m to obtain the following conserved model equations.

$$\left\{ \begin{array}{l} \frac{\partial \rho_m}{\partial t} + \frac{\partial (X_m - \rho_m p_m)}{\partial x} = 0, \\ \frac{\partial X_m}{\partial t} + \frac{\partial \left(\frac{X_m^2}{\rho_m} - p_m X_m \right)}{\partial x} = \frac{\rho_m}{\tau_m} (v_{em} - v_m), \\ \frac{\partial \rho_c}{\partial t} + \frac{\partial (X_c - \rho_c p_c)}{\partial x} = 0, \\ \frac{\partial X_c}{\partial t} + \frac{\partial \left(\frac{X_c^2}{\rho_c} - p_c X_c \right)}{\partial x} = \frac{\rho_c}{\tau_c} (v_{ec} - v_c). \end{array} \right. \quad (14)$$

In vector form, system (14) becomes

$$\frac{\partial U}{\partial t} + \frac{\partial f(U)}{\partial x} = S(U), \quad (15)$$

where

$$U = \begin{bmatrix} \rho_m \\ X_m \\ \rho_c \\ X_c \end{bmatrix}, \quad f(U) = \begin{bmatrix} X_m - \rho_m p_m \\ \frac{X_m^2}{\rho_m} - p_m X_m \\ X_c - \rho_c p_c \\ \frac{X_c^2}{\rho_c} - p_c X_c \end{bmatrix}, \quad S(U) = \begin{bmatrix} 0 \\ \frac{\rho_m}{\tau_m} (v_{em} - v_m) \\ 0 \\ \frac{\rho_c}{\tau_c} (v_{ec} - v_c) \end{bmatrix}.$$

75 3. Qualitative properties of Equilibrium velocity

We adopt a modified version of the Greenshield's equilibrium velocity

$$\left\{ \begin{array}{l} v_m^e = v_{m \max} \left(1 - \frac{AO_m}{AO_m^{\max}} \right), \text{ if } AO_m \leq AO_m^{\max}, \\ v_c^e = v_{c \max} \left(1 - \frac{AO_c}{AO_c^{\max}} \right), \text{ if } AO_c \leq AO_c^{\max}, \\ v_i^e = 0 \text{ otherwise, } i = m, c, \end{array} \right.$$

where $v_{m \max}$, $v_{c \max}$, AO_m^{\max} , AO_c^{\max} are the respective maximum velocity and maximum area occupancy of the vehicle classes. Velocities were defined in terms of AO since it is a standard measure of heterogeneous traffic concentration that lacks in lane discipline. Note that by writing AO in the form $AO_i = \psi_i \rho_i$, $i = m, c$,

80 and using definitions

$$w_m = \frac{w_c}{3} \text{ and } a_i = l_i * w_i, \quad i = m, c,$$

in (8) gives

$$v_m^e = v_{m \max} \left(1 - \frac{\rho_m [a_c (1 - \delta) + \delta a_m]}{0.85W\delta} \right). \quad (16)$$

Similarly, using (6) yields

$$v_c^e = v_{c \max} \left(1 - \frac{\rho_c [a_c (1 - \delta) + \delta a_m]}{0.74W(1 - \delta)} \right). \quad (17)$$

The dependence of equilibrium speed of the flow, v_i^e , on the area occupied by all vehicles is shown in (18) and (19) by taking derivatives of dv_c^e , with respect to AO to obtain:

$$\frac{dv_m^e}{dAO_m} = -\frac{v_{m \max}}{AO_m^{\max}}, \quad (18)$$

$$\frac{dv_c^e}{dAO_c} = -\frac{v_{c \max}}{AO_c^{\max}}. \quad (19)$$

85 From the derivatives above observe that the speed of traffic flow decreases as the area occupied by vehicles increases.

By taking derivatives with respect to the motorcycles proportion δ , we show how the speed of each vehicle class is affected by the variation in the proportion. We make use of 16 to derive

$$\frac{dv_m^e}{d\delta} = \frac{\rho_m a_c v_{m \max}}{0.85\delta^2 W}, \quad (20)$$

It is concluded from (20) that motorcycles' equilibrium speed increases with of their proportion. For the
90 case of cars, 17 is used in deriving

$$\frac{dv_c^e}{d\delta} = -\frac{a_m \rho_c v_{c \max}}{W(1 - \delta)^2}. \quad (21)$$

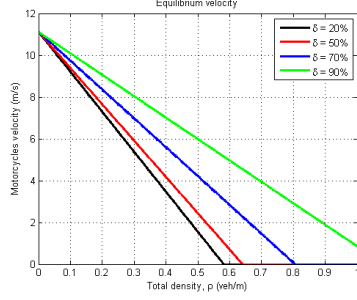
It can be deduced from (20) that an increase in motorcycles proportion leads to a decrease in velocity of cars and vice versa. Next, we look at the dynamics of equilibrium velocity when density is varied. That is achieved through derivatives

$$\frac{dv_m^e}{d\rho} = -v_{m \max} \left(\frac{[a_c (1 - \delta) + \delta a_m]}{0.85W} \right), \quad (22)$$

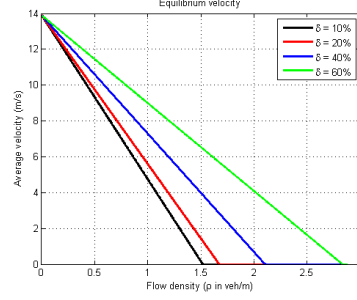
and

$$\frac{dv_c^e}{d\rho} = -v_{c \max} \left(\frac{[a_c (1 - \delta) + \delta a_m]}{0.74W} \right), \quad (23)$$

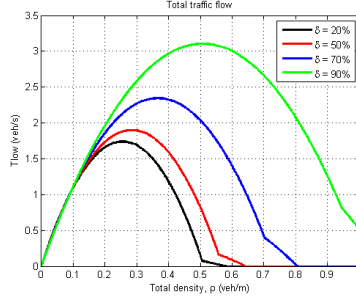
95 where $\rho_m = \delta\rho$, and $\rho_c = (1 - \delta)\rho$. It is observed from (22) and (23) that equilibrium velocity of vehicles decreases with increase of density. This behavior is further evidenced in Figure 1. In Figures 1a and 1b, cars are observed to stop much faster than motorcycles irrespective of motorcycles proportion. When the proportion is very large, motorcycles keep moving even when cars have stopped. It is because they can ably maneuver or filter through spaces unfilled by cars. Figure 1c predicts jam density reached at much earlier if
100 cars dominate the road than when motorcycles do. It can be concluded that total flow of vehicles increases with increase of motorcycles proportion.



(a) Equilibrium velocity of motorcycles vs total density



(b) Equilibrium velocity of cars vs total density



(c) Total flow vs total density

Figure 1: Equilibrium velocities and total flow of the two vehicle classes versus total density, with varying values of motorcycles' proportion, δ .

4. Discretization scheme

The proposed model (15) in a space-time domain $[0, J] \times [0, N]$ is considered. Solving it would mean evolving the solution $U(x, t)$ in time starting from the initial condition $U(x, 0)$ and subject to boundary conditions. The space and time grids are divided into J and N equally spaced grid points $x_j = j\Delta x$, $j = 0, \dots, J$ and $t^n = n\Delta t$, $n = 0, \dots, N$, of length Δx and Δt , respectively. Approximate or discrete values of $U(x, t)$, for the data given by (15) at a time step n and spatial position j , are represented by $U_j^n \equiv U(j\Delta x, n\Delta t) \equiv U(x_j, t^n)$. Next, periodic conditions are applied to the left and right boundary points U_0^n and U_J^n , respectively. Since at any time step n , the numerical solutions are obtained as either initial data values or values computed in a previous time step, a conservative finite-difference scheme is then applied to (15). Hence, the solution U_j^{n+1} , at the next time step is obtained as

$$U_j^{n+1} = U_j^n - \frac{\Delta t}{\Delta x} (F(U_j^n, U_{j+1}^n) - F(U_{j-1}^n, U_j^n)) + \Delta t S(U_j^n), \quad (24)$$

where $F(U_j^n, U_{j+1}^n)$ in (24) denotes Roe's numerical flux [17] and is given by

$$F(U_j^n, U_{j+1}^n) = \frac{1}{2} (F(U_j^n) + F(U_{j+1}^n)) - \frac{1}{2} (B(U_{j+1/2}^n) (U_{j+1}^n - U_j^n)), \quad (25)$$

where $B(U_{j+1/2}^n)$ represents the averaged Jacobian matrix of $f(U)$. For each time step, scheme (24) is implemented in two intermediate steps. Firstly, one finds

$$U_j^* = U_j^n - \frac{\Delta t}{\Delta x} (F(U_j^n, U_{j+1}^n) - F(U_{j-1}^n, U_j^n)), \quad (26)$$

115 obtained by ignoring the non-homogeneous part. Secondly, the solution U_j^{n+1} at time step t^{n+1} is found by adding the non-homogeneous part to (26). That is to say;

$$U_j^{n+1} = U_j^* + \Delta t S(U_j^n).$$

Below we describe the Roe's numerical scheme that is utilized in this work.

4.1. ~~4.1~~

The Roe decomposition scheme is used because it is capable of capturing abrupt changes or discontinuities in the data variables and providing accurate numerical solutions for traffic flow models [2]. Roe's scheme is employed purposely to transform the proposed model (11) into quasi-linear form and linearize locally by approximating the Jacobian matrix, $B(U)$ with Roe averages and in every time step, the procedure is repeated [18]. The resulting system can then approximate speed found from the eigenvalues of the averaged Jacobian matrix, as described below [18].

125 4.1.1. ~~4.1.1~~

The model equations are expressed in Quasi-linear form which is suitable for carrying out linearization. The homogeneous part of system (14) can be rewritten in quasi-linear form as

$$\frac{\partial U}{\partial t} + B(U) \frac{\partial U}{\partial x} = 0,$$

where

$$B(U) = \frac{\partial f}{\partial U},$$

$$= \begin{bmatrix} -(\gamma_m + 1)p_m & 1 & 0 & 0 \\ B_{21} & \frac{2X_m}{\rho_m} - p_m & 0 & 0 \\ 0 & 0 & -(\gamma_c + 1)p_c & 1 \\ 0 & 0 & -\left(\frac{X_c^2}{\rho_c^2} + \frac{\gamma_c p_c X_c}{\rho_c}\right) & \frac{2X_c}{\rho_c} - p_c \end{bmatrix} \quad (27)$$

is the Jacobian matrix with $B_{21} = -\left(\frac{X_m^2}{\rho_m^2} + \frac{\gamma_m p_m X_m}{\rho_m}\right)$. Next, we require eigenvalues and eigenvectors of (14) to be applied in the Roe numerical flux and entropy fix. Note that the eigenvalues are obtained from the characteristic equations of $B(U)$ and are given as follows:

$$\lambda_1(U) = v_m, \quad \lambda_2(U) = v_m - \gamma_m p_m, \quad \lambda_3(U) = v_c, \quad \lambda_4(U) = v_c - \gamma_c p_c. \quad (28)$$

The right eigenvectors corresponding to (28) are obtained as:

$$r_1 = \begin{pmatrix} 1 \\ (1 + \gamma_m)p_m + v_m \\ 0 \\ 0 \end{pmatrix}, \quad r_2 = \begin{pmatrix} 1 \\ v_m + p_m \\ 0 \\ 0 \end{pmatrix},$$

$$r_3 = \begin{pmatrix} 0 \\ 0 \\ 1 \\ (1 + \gamma_c)p_c + v_c \end{pmatrix}, \quad r_4 = \begin{pmatrix} 0 \\ 0 \\ 1 \\ v_c + p_c \end{pmatrix}. \quad (29)$$

We then proceed by applying the original Roe method to (14) in order to compute Roe averages. The detailed procedure of the method is described in the following steps [17]. Firstly, a parameter vector Z , is introduced such that U and $f(U)$ of (15) can be rewritten as

$$U = U(Z), \quad f(U) = f(U(Z)).$$

Next, the jumps

$$\Delta U = U_r - U_l, \quad \Delta f = f(U_r) - f(U_l), \quad (30)$$

are expressed in terms of the change

$$\Delta Z = Z_r - Z_l.$$

Letting the parameter vector

$$Z = \begin{bmatrix} \alpha_1 \\ \beta_1 \\ \alpha_2 \\ \beta_2 \end{bmatrix} = \begin{bmatrix} \frac{\sqrt{\rho_m}}{X_m} \\ \frac{X_m}{\sqrt{\rho_m}} \\ \frac{\sqrt{\rho_c}}{X_c} \\ \frac{X_c}{\sqrt{\rho_c}} \end{bmatrix},$$

implies that $\alpha_1^2 = \rho_m$, $X_m = \alpha_1\beta_1$, $\alpha_2^2 = \rho_c$ and $X_c = \alpha_2\beta_2$. So, the vectors $U = U(Z)$ and $f = f(Z)$ become

$$U = \begin{bmatrix} \alpha_1^2 \\ \alpha_1\beta_1 \\ \alpha_2^2 \\ \alpha_2\beta_2 \end{bmatrix}, \quad f = \begin{bmatrix} \alpha_1\beta_1 - \psi^\gamma \alpha_1^{2(1+\gamma_m)} \\ \beta_1^2 - \psi^\gamma \beta_1 \alpha_1^{(1+2\gamma_m)} \\ \alpha_2\beta_2 - \psi^\gamma \alpha_2^{2(1+\gamma_c)} \\ \beta_2^2 - \psi^\gamma \beta_2 \alpha_2^{(1+2\gamma_c)} \end{bmatrix}.$$

The averages of vector Z then become $\bar{Z} = [\bar{\alpha}_1, \bar{\beta}_1, \bar{\alpha}_2, \bar{\beta}_2]^T$. These are found by simple arithmetic averaging and obtained as:

$$\bar{Z} = \frac{1}{2} \begin{bmatrix} Z_l + Z_r \end{bmatrix} = \frac{1}{2} \begin{bmatrix} \alpha_{1l} + \alpha_{1r} \\ \beta_{1l} + \beta_{1r} \\ \alpha_{2l} + \alpha_{2r} \\ \beta_{2l} + \beta_{2r} \end{bmatrix}.$$

Following work by [17], two matrices $\bar{B} = \bar{B}(\bar{Z})$ and $\bar{C} = \bar{C}(\bar{Z})$ are computed such that the jumps ΔU and Δf in (30) are expressed in terms of the jump ΔZ . That is;

$$\Delta U = \bar{B}\Delta Z \quad \text{and} \quad \Delta f = \bar{C}\Delta Z. \quad (31)$$

145 Using (31) leads to $\Delta f = \overline{CB}^{-1} \Delta U$, and comparing it with property (C) of Theorem 1, equation (34), results into the Roe matrix $\overline{A} = \overline{CB}^{-1}$. Matrices \overline{B} and \overline{C} satisfying (31) are:

$$\overline{B} = \frac{dU}{dZ} \Big|_{\overline{Z}} = \begin{pmatrix} 2\overline{\alpha}_1 & 0 & 0 & 0 \\ \overline{\beta}_1 & \overline{\alpha}_1 & 0 & 0 \\ 0 & 0 & 2\overline{\alpha}_2 & 0 \\ 0 & 0 & \overline{\beta}_2 & \overline{\alpha}_2 \end{pmatrix},$$

whose inverse is computed by applying the usual definition

$$\overline{B}^{-1} = \frac{1}{\text{Det}(\overline{B})} \times \text{Adj}(\overline{B}) \text{ and}$$

$$\begin{aligned} \overline{C} &= f'(U(Z)) \Big|_{\overline{Z}}, \\ &= \begin{pmatrix} \overline{\beta}_1 - 2(\gamma_m + 1)\psi_m^{\gamma_m} \overline{\alpha}_1^{(1+2\gamma_m)} & \overline{\alpha}_1 & 0 & 0 \\ -(1 + 2\gamma_m)\psi_m^{\gamma_m} \overline{\beta}_1 \overline{\alpha}_1^{2\gamma_m} & \overline{C}_{22} & 0 & 0 \\ 0 & 0 & \overline{\beta}_2 - 2(\gamma_c + 1)\psi_c^{\gamma_c} \overline{\alpha}_2^{(1+2\gamma_c)} & \overline{\alpha}_2 \\ 0 & 0 & -(1 + 2\gamma_c)\psi_c^{\gamma_c} \overline{\beta}_2 \overline{\alpha}_2^{2\gamma_c} & \overline{C}_{44} \end{pmatrix}, \end{aligned}$$

where $\overline{C}_{22} = 2\overline{\beta}_1 - \psi_m^{\gamma_m} \overline{\alpha}_1^{(1+2\gamma_m)}$, $\overline{C}_{44} = 2\overline{\beta}_2 - \psi_c^{\gamma_c} \overline{\alpha}_2^{(1+2\gamma_c)}$. Therefore, the required Roe averaged matrix is

150 obtained as

$$\overline{A} = \begin{pmatrix} \overline{A}_{11} & 1 & 0 & 0 \\ \overline{A}_{21} & 2\left(\frac{\overline{\beta}_1}{\overline{\alpha}_1}\right) - \psi_m^{\gamma_m} \overline{\alpha}_1^{2\gamma_m} & 0 & 0 \\ 0 & 0 & -(1 + \gamma_c)\psi_c^{\gamma_c} \overline{\alpha}_2^{2\gamma_c} & 1 \\ 0 & 0 & \overline{A}_{43} & 2\left(\frac{\overline{\beta}_2}{\overline{\alpha}_2}\right) - \psi_c^{\gamma_c} \overline{\alpha}_2^{2\gamma_c} \end{pmatrix}, \quad (32)$$

where $\overline{A}_{11} = -(1 + \gamma_m)\psi_m^{\gamma_m} \overline{\alpha}_1^{2\gamma_m}$, $\overline{A}_{21} = -\left(\gamma_m \psi_m^{\gamma_m} \overline{\alpha}_1^{2\gamma_m} \frac{\overline{\beta}_1}{\overline{\alpha}_1} + \frac{\overline{\beta}_1^2}{\overline{\alpha}_1^2}\right)$,

$\overline{A}_{43} = -\left(\gamma_c \psi_c^{\gamma_c} \overline{\alpha}_2^{2\gamma_c} \frac{\overline{\beta}_2}{\overline{\alpha}_2} + \frac{\overline{\beta}_2^2}{\overline{\alpha}_2^2}\right)$ and $\frac{\overline{\beta}_1}{\overline{\alpha}_1}$, $\frac{\overline{\beta}_2}{\overline{\alpha}_2}$ represent the sum of Roe averaged velocity and pressure of motorcycles and cars, respectively. These are given by

$$\frac{\overline{\beta}_1}{\overline{\alpha}_1} = \frac{X_{mr}}{\sqrt{\rho_{mr}}} + \frac{X_{ml}}{\sqrt{\rho_{ml}}} = \overline{v}_m + \overline{p}_m, \quad \frac{\overline{\beta}_2}{\overline{\alpha}_2} = \frac{X_{cr}}{\sqrt{\rho_{cr}}} + \frac{X_{cl}}{\sqrt{\rho_{cl}}} = \overline{v}_c + \overline{p}_c. \quad (33)$$

Using the Roe averaged velocity, \overline{v} and pressure, \overline{p} , the data variables of the proposed model can be
155 approximated over a given road section. Comparing (32) with the matrix in (27), no averaged $\overline{\rho}$ is required. Having derived the Roe matrix, \overline{A} one ensures that it satisfies properties in Theorem 1 below.

Theorem 1 (Toro [17]). ~~Definition~~

\overline{A} ~~is~~

~~the~~

(A) ~~the~~

\overline{A} ~~is~~

$\overline{\lambda}_i = \overline{\lambda}_i(U_l, U_r)$, ~~and~~

$\overline{\lambda}_1 \leq \overline{\lambda}_2 \leq \dots \leq \overline{\lambda}_m$

160

$\overline{d} \quad \overline{r}_1, \overline{r}_2, \dots, \overline{r}_m$ ~~are~~

(B) ~~C₁~~

$$\bar{A}(U, U) = B(U).$$

(C) ~~C₂~~

$$f(U_r) - f(U_l) = \bar{A}(U_r - U_l). \quad (34)$$

Recalling the Jacobian matrix, eigenvalues and corresponding right eigenvectors of the proposed model given in (27) - (29), the averaged eigenvalues are deduced as

$$\bar{\lambda}_1(\bar{U}) = \bar{v}_m - \gamma_m \bar{p}_m, \quad \bar{\lambda}_2(\bar{U}) = \bar{v}_m, \quad \bar{\lambda}_3(\bar{U}) = \bar{v}_c - \gamma_c \bar{p}_c, \quad \bar{\lambda}_4(\bar{U}) = \bar{v}_c.$$

165 These are shown to be real. Their corresponding averaged right eigenvectors

$$\begin{aligned} \bar{r}_1 &= \begin{pmatrix} 1 \\ \bar{v}_m + \bar{p}_m \\ 0 \\ 0 \end{pmatrix}, \quad \bar{r}_2 = \begin{pmatrix} 1 \\ \bar{v}_m + (1 + \gamma_m) \bar{p}_m \\ 0 \\ 0 \end{pmatrix}, \\ \bar{r}_3 &= \begin{pmatrix} 0 \\ 0 \\ 1 \\ \bar{v}_c + \bar{p}_c \end{pmatrix}, \quad \bar{r}_4 = \begin{pmatrix} 0 \\ 0 \\ 1 \\ \bar{v}_c + (1 + \gamma_c) \bar{p}_c \end{pmatrix}, \end{aligned}$$

are checked to be linearly independent. Hence, property (A) of Theorem 1 is satisfied. Property (B), is proved by evaluating the derived Roe matrix (32) at $U = [\rho_m, X_m, \rho_c, X_c]^T$. Property (C) is proved by substituting the conserved variables into (32). To find the wave strengths, s_i we project the jump, $\Delta U = U_r - U_l$ onto the right eigenvectors and obtain

$$\begin{aligned} \Delta U &= U_r - U_l = \sum_{i=1}^4 s_i \bar{r}_i, \\ \Delta \rho_m &= \rho_{mr} - \rho_{ml} = s_1 + s_2, \\ \Delta X_m &= X_{mr} - X_{ml} = (\bar{v}_m + \bar{p}_m) s_1 + (\bar{v}_m + (1 + \gamma_m) \bar{p}_m) s_2, \\ \Delta \rho_c &= \rho_{cr} - \rho_{cl} = s_3 + s_4, \\ \Delta X_c &= X_{cr} - X_{cl} = (\bar{v}_c + \bar{p}_c) s_3 + (\bar{v}_c + (1 + \gamma_c) \bar{p}_c) s_4. \end{aligned}$$

170 The solutions s_i are verified to be

$$\begin{cases} s_1 = \Delta \rho_m - \frac{\Delta X_m - (\bar{v}_m + \bar{p}_m) \Delta \rho_m}{\gamma_m \bar{p}_m}, \\ s_2 = \frac{\Delta X_m - (\bar{v}_m + \bar{p}_m) \Delta \rho_m}{\gamma_m \bar{p}_m}, \\ s_3 = \Delta \rho_c - \frac{\Delta X_c - (\bar{v}_c + \bar{p}_c) \Delta \rho_c}{\gamma_c \bar{p}_c}, \\ s_4 = \frac{\Delta X_c - (\bar{v}_c + \bar{p}_c) \Delta \rho_c}{\gamma_c \bar{p}_c}, \end{cases} \quad (35)$$

with the obvious definitions $\Delta\rho_c = \rho_{cr} - \rho_{cl}$, $\Delta\rho_m = \rho_{mr} - \rho_{ml}$, $\Delta X_c = X_{cr} - X_{cl}$, $\Delta X_m = X_{mr} - X_{ml}$. The expressions of ΔX_m , ΔX_c are given by

$$\begin{aligned}\Delta X_m &= \Delta(\rho_m(v_m + p_m)) = \Delta(\rho_m v_m) + \Delta(\rho_m p_m), \\ \Delta X_c &= \Delta(\rho_c(v_c + p_c)) = \Delta(\rho_c v_c) + \Delta(\rho_c p_c),\end{aligned}$$

where

$$\begin{aligned}\Delta(\rho_m v_m) &= \bar{\rho}_m \Delta v_m + \bar{v}_m \Delta \rho_m + O_1(\Delta^2), \\ \Delta(\rho_m p_m) &= \bar{\rho}_m \Delta p_m + \bar{p}_m \Delta \rho_m + O_2(\Delta^2), \\ \Delta(\rho_c v_c) &= \bar{\rho}_c \Delta v_c + \bar{v}_c \Delta \rho_c + O_3(\Delta^2), \\ \Delta(\rho_c p_c) &= \bar{\rho}_c \Delta p_c + \bar{p}_c \Delta \rho_c + O_4(\Delta^2), \\ O_1(\Delta^2) &= (\rho_{mr} - \rho_{ml})(v_{mr} - \bar{v}_m) - (\rho_{ml} - \bar{\rho}_m)(v_{ml} - \bar{v}_m), \\ O_2(\Delta^2) &= (\rho_{mr} - \rho_{ml})(p_{mr} - \bar{p}_m) - (\rho_{ml} - \bar{\rho}_m)(p_{ml} - \bar{p}_m), \\ O_3(\Delta^2) &= (\rho_{cr} - \rho_{cl})(v_{cr} - \bar{v}_c) - (\rho_{cl} - \bar{\rho}_c)(v_{cl} - \bar{v}_c), \\ O_4(\Delta^2) &= (\rho_{cr} - \rho_{cl})(p_{cr} - \bar{p}_c) - (\rho_{cl} - \bar{\rho}_c)(p_{cl} - \bar{p}_c).\end{aligned}$$

Finally, using (33) – (35) into any of the expressions (25) or

$$\bar{F} = \frac{1}{2}(F_l + F_r) - \frac{1}{2} \sum_{i=1}^4 s_i |\bar{\lambda}_i| \bar{r}_i,$$

175 leads to the sought Roe numerical flux.

4.1.2. Entropy fix

In this subsection, discontinuities that develop particularly at road section boundaries are dissolved by applying an entropy condition to the Roe decomposition. By doing this, a continuous numerical solution is obtained. An entropy solution $e | \Gamma | e^{-1}$, is then substituted for the Jacobian matrix (27), where 180 $| \Gamma | = [\bar{\lambda}_1, \bar{\lambda}_2, \dots, \bar{\lambda}_K]$ refers to a diagonal matrix made up of averaged eigenvalues $\bar{\lambda}_k$, $k = 1, 2, \dots, K$ of (27), e is a matrix made up of averaged eigenvectors and e^{-1} an inverse of e [2]. Next, the eigenvalues are modified by employing Harten and Hyman entropy fix scheme in order to accurately characterize the numerical solutions [2]. Hence, the modified eigenvalues become

$$\bar{\lambda}_k = \begin{cases} \bar{\delta}_k, & \text{for } |\lambda_k| \leq \bar{\delta}_k, \\ |\bar{\delta}_k|, & \text{for } |\lambda_k| \geq \bar{\delta}_k, \end{cases}$$

where $\bar{\delta}_k = \max(0, \lambda_{j+1/2} - \lambda_j, \lambda_{j+1} - \lambda_{j+1/2})$. This ensures that the eigenvalues $\bar{\delta}_k$ are non negative 185 and have different values at the road section boundaries. However, for abrupt changes at the road section boundaries, $\bar{\delta}_k$ is set to zero. Using similar procedure as in [2], the transformed Jacobian matrix is given by $e | \Gamma | e^{-1}$, where

$$e = \left(\begin{array}{cccc} r_1 & r_2 & r_3 & r_4 \end{array} \right) \Big|_{\bar{\rho}_m, \bar{v}_m, \bar{\rho}_c, \bar{v}_c, m},$$

$$\begin{aligned}
|\Gamma| &= \begin{pmatrix} |\bar{\lambda}_1(U)| & 0 & 0 & 0 \\ 0 & |\bar{\lambda}_2(U)| & 0 & 0 \\ 0 & 0 & |\bar{\lambda}_3(U)| & 0 \\ 0 & 0 & 0 & |\bar{\lambda}_4(U)| \end{pmatrix}, \\
e^{-1} &= \begin{pmatrix} \frac{-(\bar{v}_m + \bar{p}_m)}{\gamma_m \bar{p}_m} & \frac{1}{\gamma_m \bar{p}_m} & 0 & 0 \\ \frac{\gamma_m \bar{p}_m + (\bar{v}_m + \bar{p}_m)}{\gamma_m \bar{p}_m} & \frac{-1}{\gamma_m \bar{p}_m} & 0 & 0 \\ 0 & 0 & \frac{-(\bar{v}_c + \bar{p}_c)}{\gamma_c \bar{p}_c} & \frac{1}{\gamma_c \bar{p}_c} \\ 0 & 0 & \frac{\gamma_c \bar{p}_c + (\bar{v}_c + \bar{p}_c)}{\gamma_c \bar{p}_c} & \frac{-1}{\gamma_c \bar{p}_c} \end{pmatrix}, \\
\bar{p}_m &= \psi^\gamma \left(\frac{\rho_{mr} + \rho_{mr}}{2} \right)^\gamma, \quad \bar{p}_c = \psi^\gamma \left(\frac{\rho_{cl} + \rho_{cr}}{2} \right)^\gamma,
\end{aligned}$$

The sought Roe numerical flux is finally derived by evaluating $F(U_j)$, $F(U_{j+1})$ and substituting $e|\Gamma|e^{-1}$ for $B(U_{j+1/2})$ into (25). Hence, the solutions at subsequent time steps $n+1$, are obtained using the derived flux (25) into (24). Stability of the discretization schem is established by satisfying the Courant, Friedrich and Lewy (CFL) [19].

5. Stability analysis of model equations

In this Section, behavior of the proposed traffic flow model when subjected to small disturbances is determined following the procedure outlined in [15]. To determine the model's stability, initial densities ρ_{m0} , ρ_{c0} at time t_0 and corresponding equilibrium velocities, v_{m0} , $v_{c0} = v_{em}(\psi\rho_{c0})$, $v_{ec}(\psi\rho_{c0})$ are considered [2]. The initial data is then subjected to changes (or perturbations) denoted $\sigma_{\rho_m}(x, t)$, $\sigma_{\rho_c}(x, t)$ and $\sigma_{v_m}(x, t)$, $\sigma_{v_c}(x, t)$, and given by

$$\begin{cases} \sigma_{\rho_m}(x, t) = \rho_m(x, t) - \rho_{m0}, \\ \sigma_{v_m}(x, t) = v_m(x, t) - v_{m0}, \\ \sigma_{\rho_c}(x, t) = \rho_c(x, t) - \rho_{c0}, \\ \sigma_{v_c}(x, t) = v_c(x, t) - v_{c0}. \end{cases}$$

Conditions under which changes in density and velocity grows, and eventually causes traffic congestion are determined by assuming sufficiently small changes, smooth functions and periodic functions [15]. Thus, stability of the proposed model is implied by stability of a linear combination of such functions. Hence, the changes are characterized as

$$\begin{cases} \sigma_{\rho_m}(x, t) = \rho_{m0}e^{ikx+rt}, \\ \sigma_{v_m}(x, t) = v_{m0}e^{ikx+rt}, \\ \sigma_{\rho_c}(x, t) = \rho_{c0}e^{ikx+rt}, \\ \sigma_{v_c}(x, t) = v_{c0}e^{ikx+rt}, \end{cases} \quad (36)$$

where $i = \sqrt{-1}$, r refers to frequency of oscillations, k number of changes caused by spatial evolution and kx the spatial evolution [2]. It can be inferred from (36) that traffic flow is a periodic function of kx since $e^{ikx} = \cos(kx) + i \sin(kx)$. At time t , changes in densities and velocities of motorcycles and cars are represented
205 by $\rho_{m0}e^{rt}$, $\rho_{c0}e^{rt}$, and $v_{m0}e^{rt}$, $v_{c0}e^{rt}$, respectively and rt is the growth rate of the changes. Therefore, the changes with respect to space and time become

$$\begin{aligned} \frac{\partial \sigma_{\rho c}(x, t)}{\partial x} &= ik\rho_{c0}e^{ikx+rt}, & \frac{\partial \sigma_{\rho m}(x, t)}{\partial x} &= ik\rho_{m0}e^{ikx+rt}, \\ \frac{\partial \sigma_{\rho c}(x, t)}{\partial t} &= r\rho_{c0}e^{ikx+rt}, & \frac{\partial \sigma_{\rho m}(x, t)}{\partial t} &= r\rho_{m0}e^{ikx+rt}, \\ \frac{\partial \sigma_{v c}(x, t)}{\partial x} &= ikv_{c0}e^{ikx+rt}, & \frac{\partial \sigma_{v m}(x, t)}{\partial x} &= ikv_{m0}e^{ikx+rt}, \\ \frac{\partial \sigma_{v c}(x, t)}{\partial t} &= rv_{c0}e^{ikx+rt}, & \frac{\partial \sigma_{v m}(x, t)}{\partial t} &= rv_{m0}e^{ikx+rt}. \end{aligned}$$

Suppose that a sufficiently small and smooth perturbation $(\sigma_{\rho c}, \sigma_{v c}, \sigma_{\rho m}, \sigma_{v m})$ is given to a steady-state solution $\rho_{c0}, v_{ec}(\rho_{c0}), \rho_{m0}, v_{em}(\rho_{m0})$. We then examine the effect of the parameter ψ , on the propagation of small disturbance. Substituting a small change (36) into the proposed model, using Taylor's series expansion
210 at $(\rho_{c0}, v_{c0}, \rho_{m0}, v_{m0})$, collecting linear terms where necessary and dropping all non-linear terms [15] the following linearized system is obtained:

$$\begin{cases} \frac{\partial \sigma_{\rho m}}{\partial t} + v_{m0} \frac{\partial \sigma_{\rho m}}{\partial x} + \rho_{m0} \frac{\partial \sigma_{v m}}{\partial x} = 0, \\ \frac{\partial \sigma_{v m}}{\partial t} + v_{m0} \frac{\partial \sigma_{v m}}{\partial x} + \frac{\partial p_m(\rho_{m0})}{\partial \rho_m} \frac{\partial \sigma_{\rho m}}{\partial t} + v_{m0} \frac{\partial p_m(\rho_{m0})}{\partial \rho_m} \frac{\partial \sigma_{\rho m}}{\partial x} - A_1 = 0, \\ \frac{\partial \sigma_{\rho c}}{\partial t} + v_{c0} \frac{\partial \sigma_{\rho c}}{\partial x} + \rho_{c0} \frac{\partial \sigma_{v c}}{\partial x} = 0, \\ \frac{\partial \sigma_{v c}}{\partial t} + v_{c0} \frac{\partial \sigma_{v c}}{\partial x} + \frac{\partial p_c(\rho_{c0})}{\partial \rho_c} \frac{\partial \sigma_{\rho c}}{\partial t} + v_{c0} \frac{\partial p_c(\rho_{c0})}{\partial \rho_c} \frac{\partial \sigma_{\rho c}}{\partial x} - A_2 = 0, \end{cases} \quad (37)$$

where $A_1 = \frac{\psi_m v'_{em}(\psi_m \rho_{m0}) \sigma_{\rho m} - \sigma_{v m}}{\tau_c}$, $A_2 = \frac{\psi_c v'_{ec}(\psi_c \rho_{c0}) \sigma_{\rho c} - \sigma_{v c}}{\tau_c}$. Following [15], we assume that

$$\frac{\sigma_{\rho c}(x, t)}{\rho_{c0}} \ll 1, \quad \frac{\sigma_{\rho m}(x, t)}{\rho_{m0}} \ll 1, \quad \frac{\sigma_{v c}(x, t)}{v_{c0}} \ll 1, \quad \frac{\sigma_{v m}(x, t)}{v_{m0}} \ll 1.$$

Hence, system (37) simplifies to

$$\begin{cases} r\sigma_{\rho m} + v_{m0} ik \sigma_{\rho m} + \rho_{m0} ik \sigma_{v m} = 0, \\ r\sigma_{v m} + v_{m0} ik \sigma_{v m} + r \frac{\partial p_m(\rho_{c0})}{\partial \rho_m} \sigma_{\rho m} + v_{m0} ik \frac{\partial p_m(\rho_{m0})}{\partial \rho_m} \sigma_{\rho m} - A_2 = 0, \\ r\sigma_{\rho c} + v_{c0} ik \sigma_{\rho c} + \rho_{c0} ik \sigma_{v c} = 0, \\ r\sigma_{v c} + v_{c0} ik \sigma_{v c} + r \frac{\partial p_c(\rho_{c0})}{\partial \rho_c} \sigma_{\rho c} + v_{c0} ik \frac{\partial p_c(\rho_{c0})}{\partial \rho_c} \sigma_{\rho c} - A_1 = 0. \end{cases}$$

The resulting Jacobian matrix, J is given by

$$\begin{bmatrix} r + v_{c0} ik & \rho_{c0} ik & 0 & 0 \\ (r + v_{c0} ik) \frac{\partial p_c(\rho_{c0})}{\partial \rho_c} - \frac{\psi_c v'_{ec}(\psi_c \rho_{c0})}{\tau_c} & r + v_{c0} ik + \frac{1}{\tau_c} & 0 & 0 \\ 0 & 0 & r + v_{m0} ik & \rho_{m0} ik \\ 0 & 0 & J_{43} & J_{44} \end{bmatrix},$$

215 where $J_{43} = (r + v_{m0}ik) \frac{\partial p_m(\rho_{c0})}{\partial \rho_m} - \frac{\psi_m v'_{em}(\psi_m \rho_{m0})}{\tau_m}$, $J_{44} = r + v_{m0}ik + \frac{1}{\tau_m}$. For non-trivial solutions, $\det(J) = 0$. Thus, the solutions of $J(\sigma_{\rho_c}, \sigma_{v_c}, \sigma_{\rho_m}, \sigma_{v_m}) = 0$ are denoted $r_{1\pm}$, $r_{2\pm}$, respectively and given by

$$\frac{\frac{\partial p_m}{\partial \rho_m} ik \rho_{m0} \tau_m - 2ik \tau_m v_{m0} - 1 \pm \sqrt{G}}{2\tau_m}, \frac{\frac{\partial p_c}{\partial \rho_c} ik \rho_{c0} \tau_c - 2ik \tau_c v_{c0} - 1 \pm \sqrt{G}}{2\tau_c},$$

where

$$G = \left(\frac{\partial p_m}{\partial \rho_m} \right)^2 i^2 k^2 \rho_{m0}^2 \tau_m^2 - 4\psi_m ik \rho_{m0} \tau_m v'_{em} - 2 \frac{\partial p_m}{\partial \rho_m} ik \rho_{m0} \tau_m + 1.$$

For stability of the proposed model, changes in densities and velocities need to decrease as time progresses.

Hence, the real parts $Re(r_{1\pm}, r_{2\pm})$, of $\det(J)$ must be strictly negative. That is to say; $Re(r_{1\pm}), Re(r_{2\pm}) < 0$.

220 However, the square root contains a complex number. So, it becomes difficult to determine the sign. Hence, we apply the formula [20]

$$\sqrt{R \pm i|I|} = \sqrt{\frac{1}{2} \left(\sqrt{R^2 + I^2} + R \right)} \pm i \sqrt{\frac{1}{2} \left(\sqrt{R^2 + I^2} - R \right)}, \quad (38)$$

where

$$\begin{aligned} R_c &= 1 - \left(\frac{\partial p_c(\rho_{c0})}{\partial \rho_c} \right)^2 k^2 \rho_{c0}^2 \tau_c^2, \quad I_c = 4\psi_c k \rho_{c0} \tau_c v'_{ec} + 2 \frac{\partial p_c}{\partial \rho_c} k \rho_{c0} \tau_c, \\ R_m &= 1 - \left(\frac{\partial p_m(\rho_{m0})}{\partial \rho_m} \right)^2 k^2 \rho_{m0}^2 \tau_m^2, \quad I_m = 4\psi_m k \rho_{m0} \tau_m v'_{em} + 2 \frac{\partial p_m}{\partial \rho_m} k \rho_{m0} \tau_m. \end{aligned}$$

Let us consider $Re(r_{1+})$. To have $Re(r_{1+}) < 0$, would mean

$$-1 + \sqrt{\frac{1}{2} \left(\sqrt{R_m^2 + I_m^2} + R_m \right)} < 0.$$

After simplifying and substituting for R_m and I_m of (38) into the previous the stability condition is derived

225 as

$$\psi_m v'_{em} < -\frac{\partial p_m}{\partial \rho_m}. \quad (39)$$

In the same way, the stability condition can be derived for $Re(r_{2+}) < 0$ and obtained as

$$\psi_c v'_{em} < -\frac{\partial p_c}{\partial \rho_c}. \quad (40)$$

Data for the proposed model is chosen such that it satisfies the stability conditions in (39) and (40).

6. Numerical results

The following subsections describe vehicles' density, velocity and flow distributions when motorcycles' proportion is set to 20% and 90%. Considering (2) and (10), we look at freeway and congested traffic on roundabout. Roe's numerical scheme is utilized in which periodic boundary conditions are applied in order to represent a circular road. In an attempt to dissolve discontinuities at boundaries, an entropy fix is applied to the Roe's numerical scheme. Stability of the scheme is established by applying CFL stability condition. Table 1 shows parameter values that are used for simulations. Note that when δ takes on values 0 and 1, 230 results become unstable (undefined). Figures 2 - 6 display simulation results of the proposed model. 235

Table 1: Simulation parameters.

Description	Value	Source
Length of the road	200m	
Road step, h	5 m	[2]
Time step	0.05 s	
Relaxation time, τ_m, τ_c	2s, 2.5s	[2]
Equilibrium velocity $v_e(\rho_m), v_e(\rho_c)$	Greenshields	[2]
Maximum normalized density	$\rho = \rho_m + \rho_c = 1$	[2]
Maximum speed, $v_{m \max}$	11m/s	[21]
Maximum speed, $v_{c \max}$	13.8m/s	[22]
Maximum area occupancy, AO_m^{\max}	0.85	[23]
Maximum area occupancy, AO_c^{\max}	0.74	[23]
$\gamma_i, i = m, c$	2.23, 2.12	[23]
Width of the road	12m	[22]
Width of a car	1.6m	[24]
Vehicle class proportion, δ	20%, 90%	
Length of a car	4m	[24]
Length of a motorcycle	1.8m	[24]
Simulation time, T	60 seconds	[2]

6.1. Efficiency

Under this subsection, we consider a free traffic flow with motorcycles proportion δ , initially fixed at 20%, for 0s, 1s, 20s, 40s and 60s. The initial total density of traffic flow denoted ρ_0 , is set to be

$$\rho_0 = \begin{cases} 0.1, & \text{for } x < 100 \\ 0.2, & \text{for } x \geq 100. \end{cases} \quad (41)$$

Since $\delta = 20\%$ it follows that $\rho_m = 0.2\rho_0$ and $\rho_c = 0.8\rho_0$. The initial density distributions of the respective vehicle classes are plotted in Figure 2a, and corresponding velocities depicted by Figure 2b. In Figure 2, a shock wave develops at 1s for both vehicle classes at 100m (when the low density stream meets high density stream). After 20s, the shock wave is smoothed and both vehicle classes move with velocities close to their respective maximum values. That is; 13.8m/s and 11m/s for cars and motorcycles, respectively (see Figures 2f - 2j). Next, δ is set to 90%, such that $\rho_m = 0.9\rho_0$ and $\rho_c = 0.1\rho_0$, for motorcycles and cars, respectively. The plot of such initial density profile is shown in Figure 3a with corresponding velocities in Figure 3b. Same results are observed when $\delta = 90\%$ (see Figures 3f - 3j) Therefore, it can be concluded that there is minimal effect of motorcycles proportion during freeway traffic flow.

6.2. Congestion

Now we consider a congested 200m circular road with total initial density, ρ_0 given by

$$\rho_0 = \begin{cases} 0.3, & \text{if } x \leq 130 \\ 0.6, & \text{if } 130 < x < 180 \\ 0.1, & \text{if } x \geq 180. \end{cases} \quad (42)$$

The proposed model densities and velocities at time, $T = 0s, 1s, 20s, 40s$ and 60s, with δ initially fixed at 20% are displayed in Figure 4. Plots of initial densities and velocities are displayed by Figures 4a and 4b, respectively. It is observed in Figures 4c - 4j that at all selected times, both vehicle classes develop shock waves as high and low densities of vehicles meet. However, the shock waves are smoothed at 20s and beyond, since an entropy fix is applied to Roe numerical scheme. We further observe that velocities for both vehicle classes decrease far away from their maximum values as time progresses. Different from the freeway traffic flow scenario, velocities of both vehicle classes are non uniform at all times since they are congested. Cars form a rarefaction wave at $T = 1s$ and 180m, but propagates to the left at 20s and 40s and later disappears at 60s. A rarefaction wave develops for motorcycles at $T = 1s$ and 180m but disappears at 20s. A shock wave develops for both vehicle classes at $T = 1s$ and 130m, but for cars it propagates to the left at 20s and 40s and later moves back to the right at 60s. At 20s and 60s, motorcycles hit jam before cars. At 40s, cars hit jam faster than motorcycles. At any time, jam is created in one region for cars while motorcycles density is maintained at low values.

Next δ is set to be 90%, that is; fewer cars and many motorcycles. The initial density and velocity distributions are indicated in Figures 5a and 5b. Density for cars is observed to be almost uniform after 1s

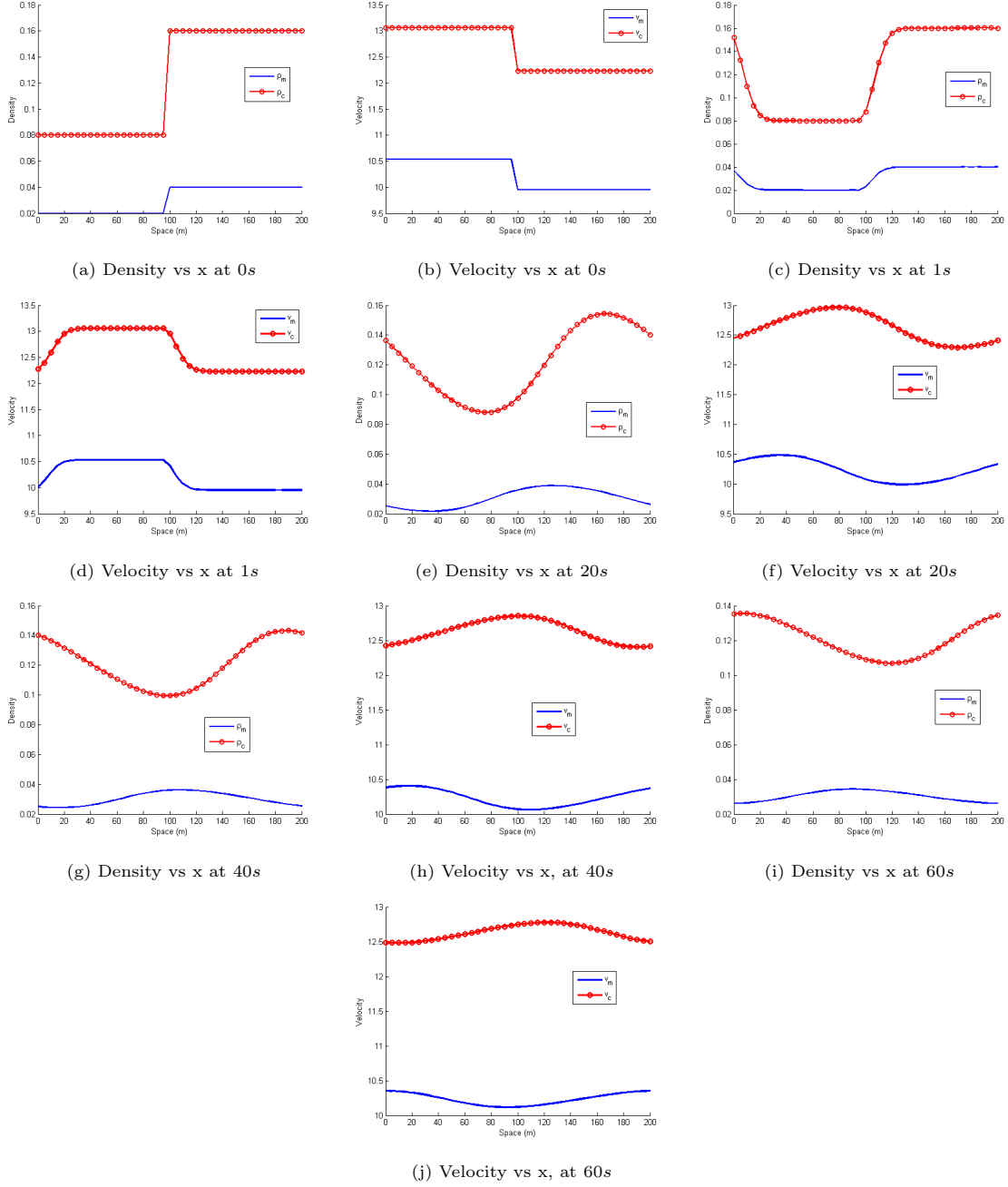


Figure 2: Densities and velocities of the proposed model on a 200m freeway circular road when $\delta = 20\%$, at $T = 0s, 1s, 20s, 40s$ and 60s.

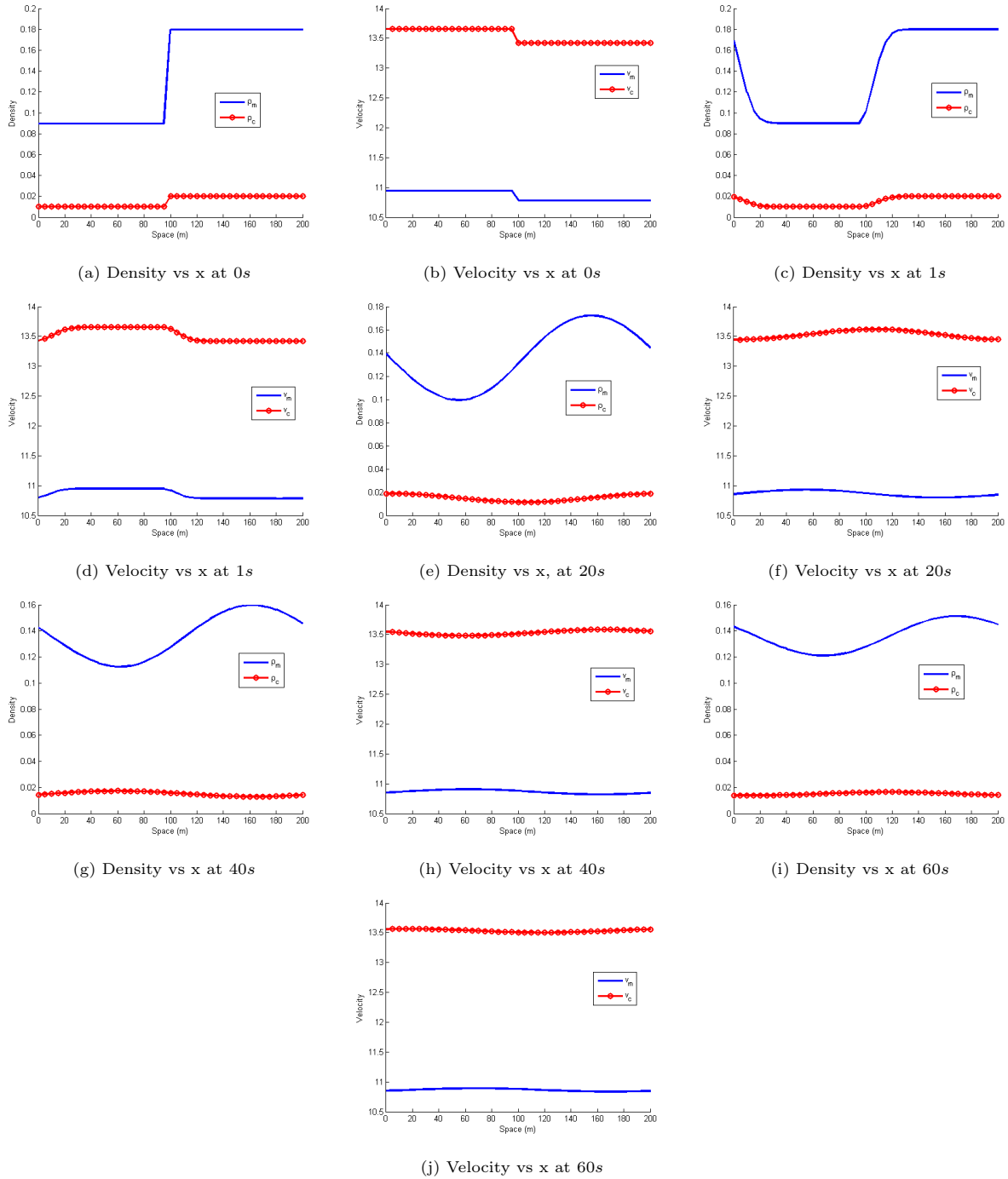


Figure 3: Densities and velocities of the proposed model on a 200m freeway circular road when $\delta = 90\%$, at $T = 0s, 1s, 20s, 40s$ and 60s.

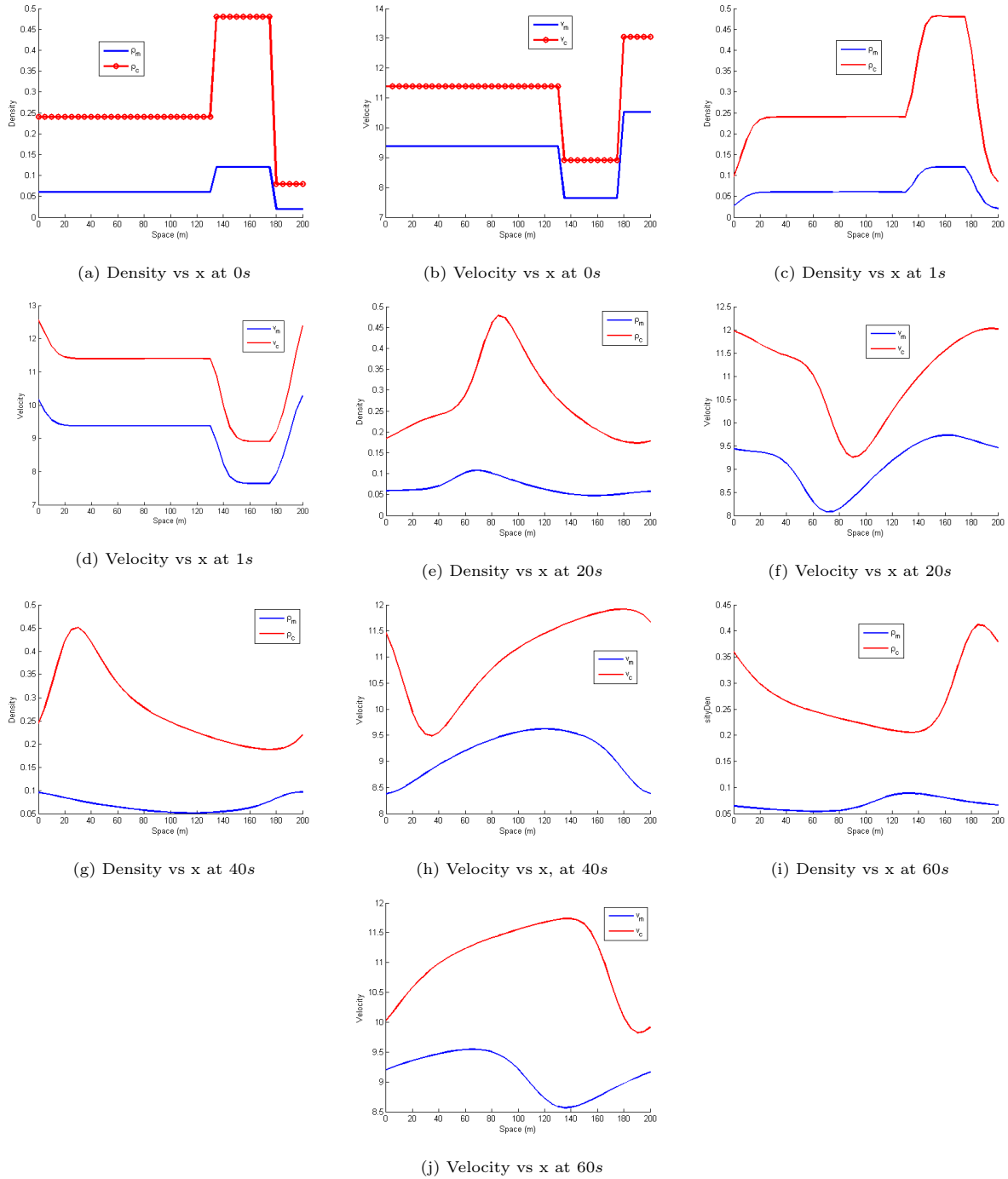


Figure 4: Densities and velocities of the proposed model on a 200m congested circular road when $\delta = 20\%$, at time $T = 0s, 1s, 20s, 40s$ and $60s$.

while for motorcycles is non uniform at all times. A shock wave is shown to clear faster for cars than for motorcycles. A stationary shock wave but with decreasing amplitude develops for motorcycles in one region after 1s, where they find difficulties squeezing through spaces unfilled by the many cars. Figures 6a - 6h display the space-time evolution of densities and velocities for both vehicle classes, when $\delta = 20\%$ and 90% . The densities and velocities become smooth as time progresses.

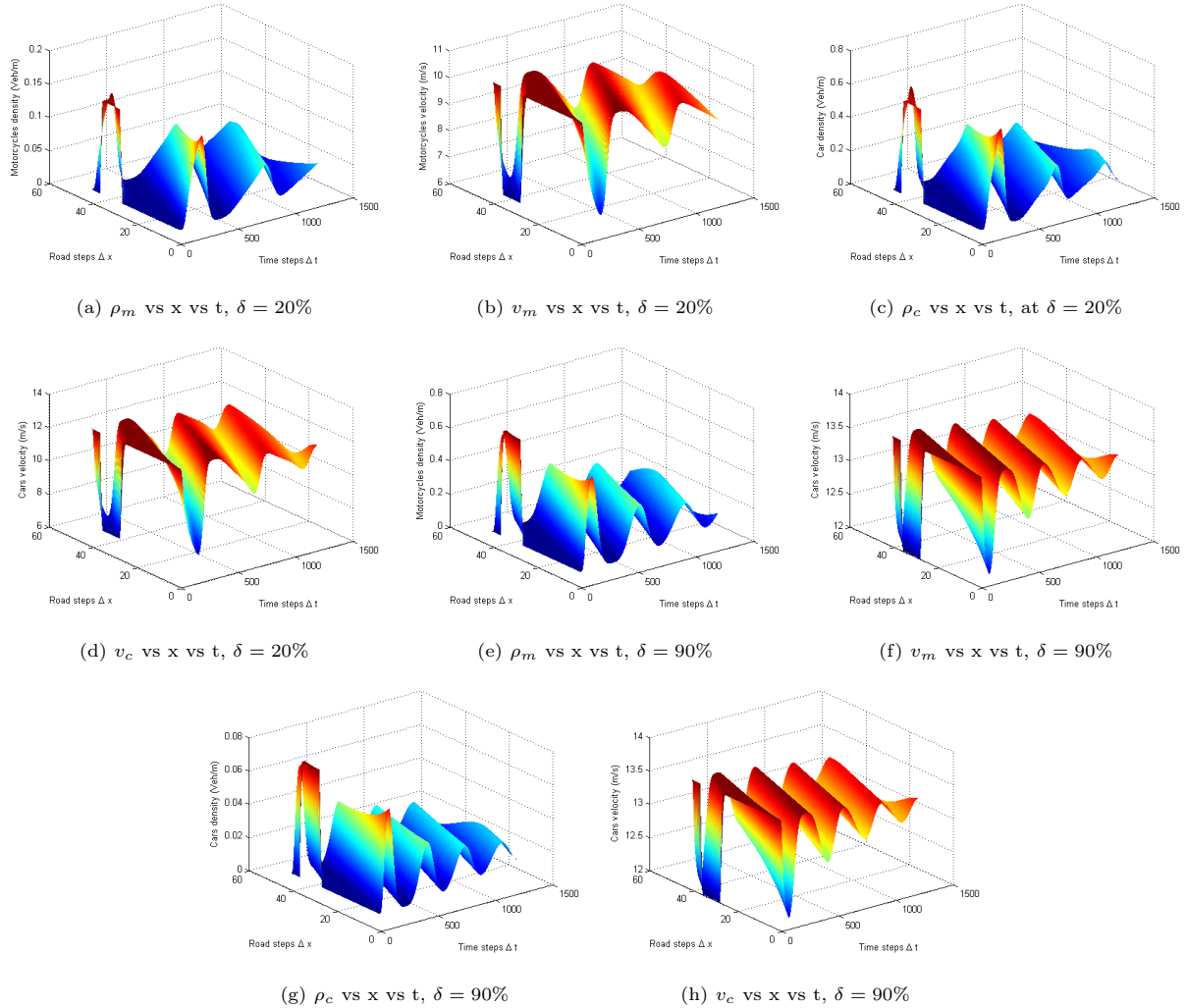


Figure 6: Densities and velocities of the proposed model on a 200m congested circular road when $\delta = 20\%$ and 90% , at 60s.

7. Conclusion

The aim of this paper is to determine the effect of proportional densities on the flow of traffic. A new expression for area occupancy, defined in terms of proportion densities is proposed. Roe's scheme is explicitly applied, where Roe matrix, averaged velocity, averaged pressure, wave strengths are derived. An entropy condition is applied to Roe decomposition. Stability conditions for each vehicle class are obtained by linear stability analysis whereas stability of the numerical scheme is determined by the CFL condition.

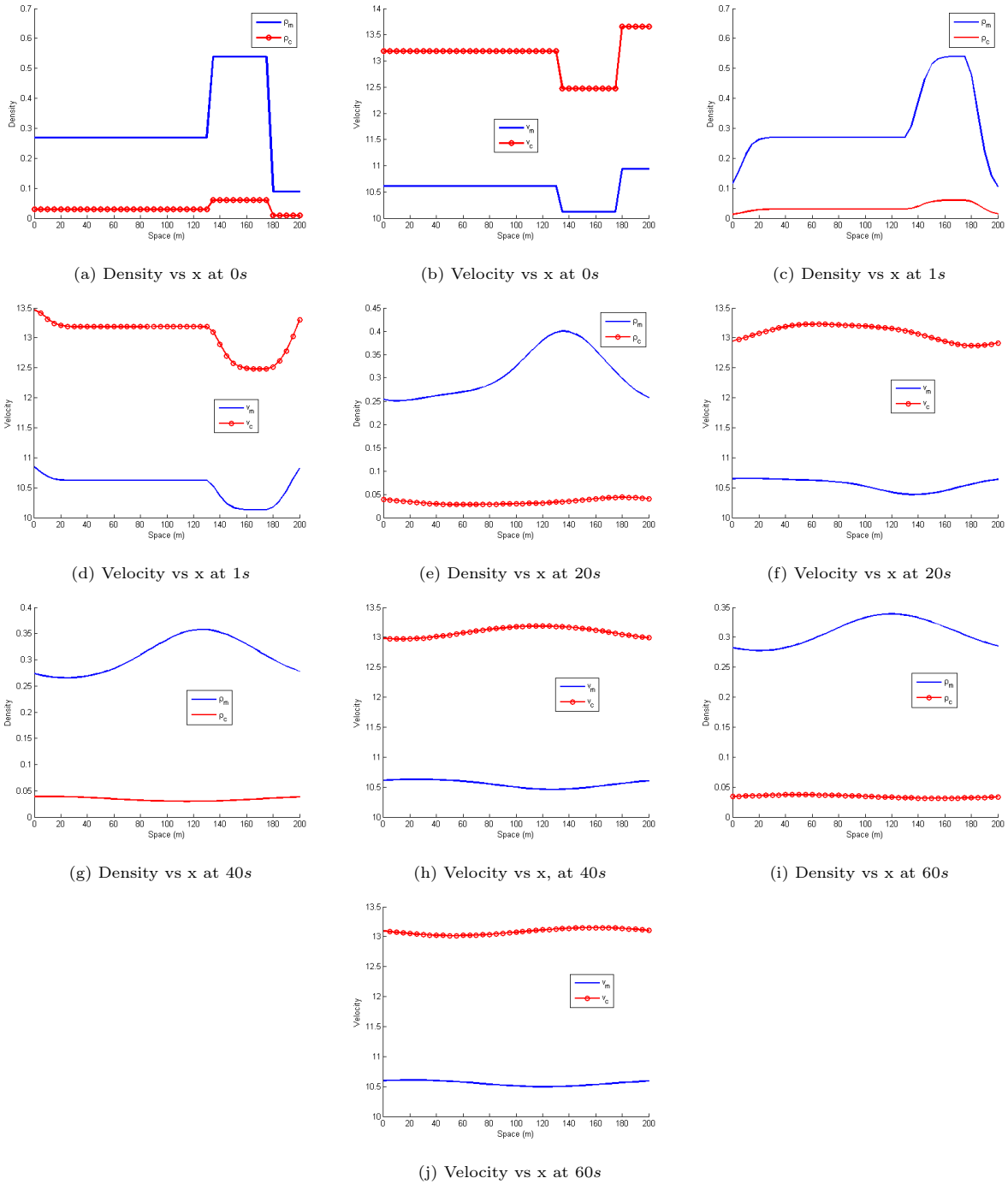


Figure 5: Densities and velocities of the proposed model on a 200m congested circular road when $\delta = 90\%$, at 0s, 1s, 20s, 40s and 60s.

Qualitative analysis shows that Roe decomposition scheme can be applied to AR model and other variants. Numerical results show that when motorcycles are more than cars, all vehicle classes move with higher velocities than when motorcycles are fewer. A shock wave is observed to clear faster for cars than for motorcycles since motorcycles are slower than cars. On the other hand if motorcycles are fewer than cars, both vehicle classes develop shock waves but this effect is more felt during congested traffic flow. Traffic jam is shown to occur much earlier if cars dominate the road than when motorcycles do. At any time, whenever cars develop shock wave motorcycles too develop the shock. Densities and velocities for each vehicle class become smoother over time and were shown to remain within limits. Thus, the results obtained from the proposed model are realistic. Total traffic flow increases with increase of motorcycles proportion. As a control for traffic jam, enforcement of lane discipline is recommended.

Acknowledgment

The first author acknowledges her other research supervisors Prof. J.Y.T Mugisha of Department of Mathematics, Makerere University, P.O Box 7062, Kampala, Uganda and Prof. Semu Mitiku Kassa of Department of Mathematics and Statistical Sciences, Botswana International University of Science and Technology (BIUST), P/Bag 16, Palapye, Botswana for providing technical guidance and mentorship. The first author also acknowledges the Sida bilateral program with Makerere University, 2015-2020, project 316 “Capacity building in Mathematics and its applications” for providing financial support.

References

- [1] Y. Li, D. Sun, Microscopic car-following model for the traffic flow: the state of the art, *Journal of Control Theory and Applications* 10 (2) (2012) 133–143.
- [2] Z. H. Khan, W. Imran, S. Azeem, K. S. Khattak, T. A. Gulliver, M. S. Aslam, A macroscopic traffic model based on driver reaction and traffic stimuli, *Applied Sciences* 9 (14) (2019) 2848.
- [3] D. P. Moller, *Introduction to Transportation Analysis, Modeling and Simulation: Computational Foundations and Multimodal Applications*, Springer, London, 2014.
- [4] S. Maerivoet, B. De Moor, Transportation planning and traffic flow models, arXiv preprint physics/0507127.
- [5] V. Knoop, *Introduction to traffic flow theory: An introduction with exercises*.
- [6] M. J. Lighthill, G. B. Whitham, On kinematic waves II. A theory of traffic flow on long crowded roads, *Proceedings of the Royal Society of London. Series A. Mathematical and Physical Sciences* 229 (1178) (1955) 317–345.
- [7] P. I. Richards, Shock waves on the highway, *Operations research* 4 (1) (1956) 42–51.

- [8] S. Fan, D. B. Work, A heterogeneous multiclass traffic flow model with creeping, *SIAM J. Appl. Math.* 75 (2015) 813–835.
- [9] R. Nair, H. S. Mahmassani, E. Miller-Hooks, A porous flow approach to modeling heterogeneous traffic
310 in disordered systems, *Procedia-Social and Behavioral Sciences* 17 (2011) 611–627.
- [10] S. Gashaw, P. Goatin, J. Härrri, Modeling and analysis of mixed flow of cars and powered two wheelers, *Transportation Research Part C: Emerging Technologies* 89 (2018) 148–167. doi:10.1016/j.trc.2018.02.004.
- [11] J. Hawkins, L. Kattan, Microsimulating heterogeneous traffic: An implementation of the porous flow
315 approach, *Transportation in Developing Economies* 4 (2018) 1–12.
- [12] R. Mohan, G. Ramadurai, Heterogeneous traffic flow modelling using macroscopic continuum model, *Procedia-Social and Behavioral Sciences* 104 (2013) 402–411.
- [13] H. J. Payne, Models of freeway traffic and control, in: *Mathematical Models of Public Systems*, ed. by G.A. Bekey (Simulation Council, La Jolla), Vol. 1, Simulation Council, Inc., 1971, pp. 51 – 61.
- [14] H. J. Payne, FREFLO: A macroscopic simulation model of freeway traffic, *Transportation Research Record* 722 (1979) 68 – 77.
320
- [15] A. K. Gupta, I. Dhiman, Analyses of a continuum traffic flow model for a nonlane-based system, *International Journal of Modern Physics C* 25 (10) (2014) 1450045.
- [16] R. Mohan, G. Ramadurai, Heterogeneous traffic flow modelling using second-order macroscopic contin-
325 uum model, *Physics Letters A* 381 (3) (2017) 115–123. doi:10.1016/j.physleta.2016.10.042.
- [17] E. F. Toro, *Riemann solvers and numerical methods for fluid dynamics: a practical introduction*, Springer Science & Business Media, German, 2013.
- [18] P. Kachroo, S. J. Al-Nasur, S. A. Wadoo, A. Shende, *Pedestrian dynamics: Feedback control of crowd evacuation*, Springer Science & Business Media, 2008.
- [19] R. J. LeVeque, R. J. Leveque, *Numerical methods for conservation laws*, Vol. 214, Springer, 1992.
330
- [20] D. Helbing, A. Johansson, On the controversy around daganzo’s requiem for and aw-rasclé’s resurrection of second-order traffic flow models, in: *Modelling and Optimisation of Flows on Networks*, Springer, 2013, pp. 271–302.
- [21] R. Mohan, G. Ramadurai, Heterogeneous traffic flow modelling using second-order macroscopic contin-
335 uum model, *Physics Letters A* 381 (3) (2017) 115–123.
- [22] Ministry of works and transport, *Uganda road design manual 1* (2010) 190–204.

- [23] R. Mohan, Multi-class AR model: comparison with microsimulation model for traffic flow variables at network level of interest and the two-dimensional formulation, *International Journal of Modelling and Simulation* 41 (2) (2021) 81–91.
- ³⁴⁰ [24] V. T. Arasan, G. Dhivya, Measuring heterogeneous traffic density, in: *Proceedings of International Conference on Sustainable Urban Transport and Environment*, World Academy of Science, Engineering and technology, Bangkok, Vol. 36, 2008, p. 342.